Final Summary Overview: NIJ #2014-DN-BX-K005

Three-Dimensional Craniofacial Variation of Modern Americans: A Visual Reference to Supplement Facial Approximation Methods

Terrie Simmons-Ehrhardt, Catyana Falsetti, Christopher Ehrhardt

I. Purpose

The purpose of this study was to utilize computed tomography (CT) data to collect detailed measurements of the relationships between the craniofacial skeleton and soft tissues of the face to improve craniofacial identification methods in the United States. The project involved a collaborative effort between forensic science researchers and a facial approximation practitioner to produce data and resources relevant to practitioners.

II. Project Subjects

CT scans containing craniofacial data were identified from The Cancer Imaging Archives (TCIA) public database (www.cancerimagingarchive.net) [1]. Scans were downloaded from multiple collections: [2] [3] [4] [5] [6]. The entire sample consisted of 106 individuals (43 females and 63 males), but only 102 (Table 1) were subjected to landmark collection.

Table 1. Sample of unique scans used for landmark collection

			Age			
	n	n (with age)	Min	Max	Ave	SD
Females	40	37	21	80	58.6	11.2
Males	62	59	39	82	55.2	9.2

III. Project Design and Methods

CT scans were imported into Mimics v. 17.0 (Materialise, Leuven, Belgium) for segmentation and 3D reconstruction, and those of acceptable quality for measurements were retained and processed to produce clean, high resolution stereolithography models. The "Optimal" setting was found to produce inadequate 3D surface models, so a custom setting

utilizing Gray Value Interpolation was instead applied to produce the highest possible resolution models. Landmarks were placed on the 3D bone and skin models in Mimics utilizing the Simulation Module. Intraobserver error was evaluated through triplicate landmark placement on 10 heads.

Landmark coordinates were exported from Mimics and transformed to align head models to a standard orientation and coordinate system (CS) along three reference planes: the Frankfurt Horizontal (FH) plane through left orbitale (Or), left and right porion (Po); a coronal plane through left and right Po, and a mid-sagittal plane through nasion (N); resulting in the following CS: x-axis representing the medial-lateral direction (anatomical left of N = positive; N at x = 0), y-axis representing the anterior-posterior direction (anterior to coronal plane = negative; Po at y = 0), and z-axis representing the superior-inferior direction (superior to FH = positive; Or, Po at z = 0). The CS allowed us to collect measurements across a single axis, in 2D, or in 3D in views consistent with craniofacial identification methods (frontal and profile). The transformation was applied in Meshlab [7] to the 3D bone and skin models and the 3D landmark coordinates using an Excel spreadsheet. The spreadsheet and Meshlab scripts for performing this transformation have been made available for download from Figshare [8] to facilitate transformation of any 3D CT head models by other researchers.

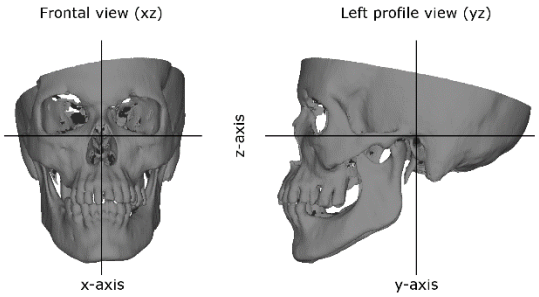

Figure 1. Orientation and coordinate system

A method for dense facial tissue depth mapping (FTDM) was developed and applied using a distance algorithm in Meshlab to generate a colorized map of distances between the skin

and craniofacial skeleton to 106 individuals, including some with more than one CT scan (total n = 112), to make intra-individual comparisons based on visually assessed relative weight (normal, thin, heavy). The distances were mapped on an RGB scale from thinnest (0.0 mm, red) to thickest (40.0 mm, blue) on both the bone and skin and can be fully visualized and interacted with in Meshlab. The steps have been detailed in a user guide that can be downloaded from Figshare [9] (Figure 2). We also "split" the depth maps into 1.0 mm increments to facilitate viewing of specific depth values. Our method can be applied to any head CT models, including cone-beam CT and is further described in a publication, a special issue of Human Biology titled "Thinking Computationally About Forensics" [10].

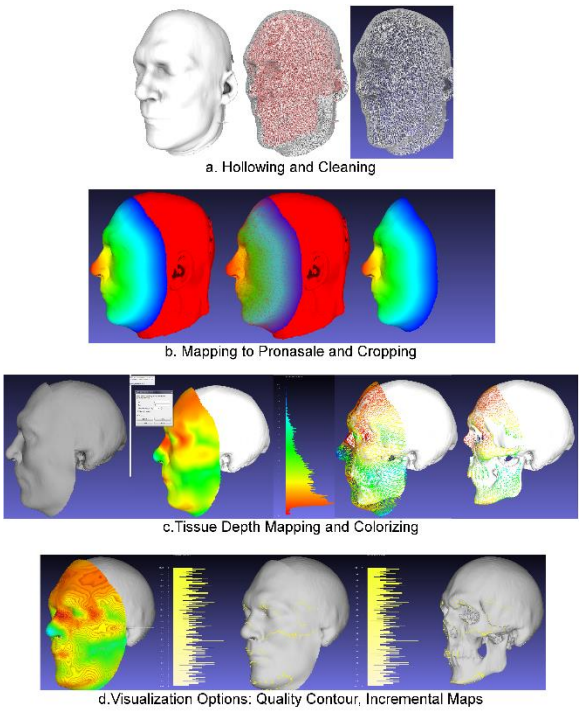

Figure 2. Summary of FTDM method

Visual observations were made primarily by the project consultant, Catyana Falsetti, a practicing forensic artist, and included comparisons of various aspects of facial features to traditional facial approximation guidelines.

IV. Data Analysis

Bone and skin interlandmark distances (ILDs) were generated with Excel and PAST v. 2.17c [11] in a single axis, 2D, and 3D and evaluated for correlations. We also evaluated positional relationships between bone and skin landmarks to find consistent associations, by assessing distances in a particular axis for non-significant differences from zero, small ranges or standard deviations, or consistent direction as indicated by coordinate signs. Statistics were

performed in Microsoft Excel, PAST v. 2.17c [11] and SPSS v. 24 (IBM). Paired t-tests were also used to test for no significant difference between bone and skin ILDs.

V. Findings

The qualitative observations indicated many discrepancies with traditional facial approximation guidelines. The analysis of landmark positions relative to bone landmarks provided quantitative evidence for new relationships. Manuscripts for each facial area are being submitted to the Journal of Forensic Sciences.

Facial Tissue Depth Mapping (FTDM)

The dense FTDMs showed that the thinnest tissues occurred most frequently on the sides and top of the nasal bones, lateral orbital margins, and forehead superior to the supraorbital border. Minimum depths ranged from 1.2 to 3.4 mm, indicating common starting depths for a face regardless of weight. Intra-individual comparisons of tissue depth maps showed that tissue depths did not increase over the entire face with increased weight, and that areas of "thin" tissues were not necessarily thicker in heavier scans.

A few individuals with thicker tissues over the nasal bones (> 3.0 mm) suggested the potential influence of nasal bone morphology on depths.

Eyes

The most projecting point of the eye, oculus anterius (Oa'), was most frequently and on average located lateral to the halfway point

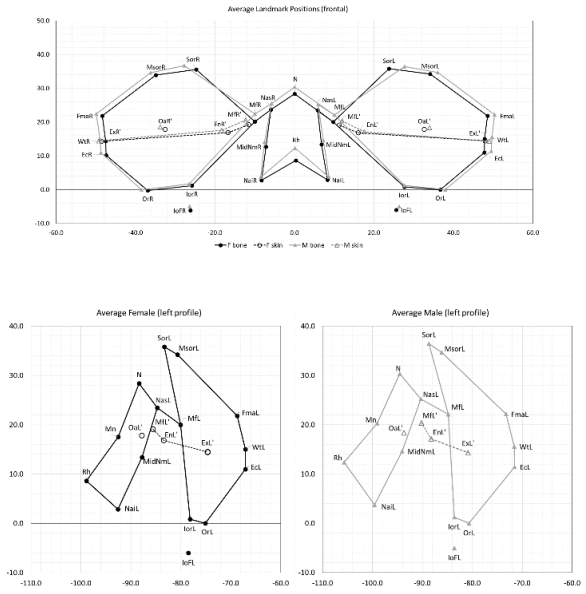

Figure 3. Average eye landmark positions

This resource was prepared by the author(s) using Federal funds provided by the U.S. Department of Justice. Opinions or points of view expressed are those of the author(s) and do not necessarily reflect the official position or policies of the U.S. Department of Justice.

between maxillofrontale and ectoconchion (female left: 3.9 mm lateral (SD = 1.4 mm); male left: 4.2 mm lateral (SD = 1.6 mm)), rather than centrally located. In addition, Oa' was always lateral to the infraorbital foramen (IoF) (excluding 1 case at 0.3 mm), medial to Or, and most frequently and on average medial to a point on the supraorbital border (Msor); anterior to the lateral and inferior orbit landmarks, anterior to Mf and Msor, with the smallest average y-axis distance to mid-nasomaxillary suture (MidNm) (females = 0.1 mm anterior, males = 0.3 mm posterior); always superior to Ec, most frequently and on average superior to Whitnall's tubercle and most frequently and on average inferior to Frontomalare anterior and Mf, with the smallest average z-axis distance to the mid-nasal point (Mn) (Figure 3). Regressions were generated based on correlations, intraobserver landmark error, and practicality of measurement collection (Table 2, Figure 4).

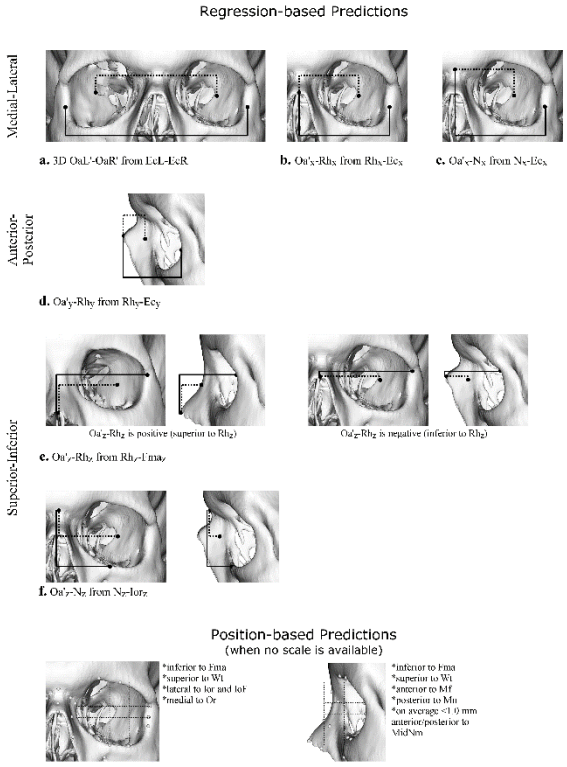

Figure 4. Prediction of Oa'

Table 2. Regression equations for predicting the position of Oa'

Position		r	r^2	Standard Error	Equation
Medial-Lateral (3D)	OaL'-OaR'	0.806	0.650	2.657	-15.532 + 0.848*(EcL-EcR)
Medial-Lateral (x)	Oa'_x-Rh_x	0.801	0.641	1.492	-7.330 + 0.835*(Rh_x-Ec_x)
Medial-Lateral (x)	Oa'_x-N_x	0.791	0.626	1.497	-7.456 + 0.838*(N_x-Ec_x)
Anterior-Posterior (y)	Oa'_y-Rh_y	0.705	0.497	2.399	-11.136 + 0.685*(Rh_y-Ec_y)
Superior-Inferior (z)	Oa'_z-Rh_z	0.871	0.758	1.801	-1.995 + 0.831*(Rh_z-Fma_z)
Superior-Inferior (z)	Oa'_z-N_z	0.745	0.555	1.531	-7.824 + 0.676*(N_z-Ior_z)

Mouth

Dental artifacts and a high frequency of tooth loss with varying degrees of alveolar resorption greatly reduced our sample for mouth measurements. Mouth width was larger in males (dentate = 57.2 mm, edentulous = 56.1 mm) than females (dentate = 53.3 mm, edentulous = 52.0 mm). A close association with IoF was found for the corners of the mouth and mouth width: female mouth width was not significantly different from infraorbital foramen width (IoFL-IoFR) (mean diff = 1.4 mm), whereas male mouth width significantly exceeded IoFL-IoFR by 4.0 mm. Mouth width exceeded distal canine width by 7.6 to 26.4 mm. Crista philtri width was not significantly different from nasospinale width in females (mean diff = 0.1 mm), but was 1.0 mm larger in males. Females had larger mean values than males for upper, lower, and total vermilion lip heights, whereas males had larger values for cutaneous lip heights to subnasale (Sn) and sublabiale (Sl) as well as larger values for all vertical bone ILDs of the mouth. Vertical mouth heights and positions did not match facial approximation guidelines: labiale superius (Ls) was nearly always inferior to prosthion/supradentale (Pr) and superior to incision (Inc), upper vermilion height was always smaller than upper enamel height (females = -5.7 mm, males = -6.4 mm), stomion (Sto) was most frequently and on average superior to Inc, and labiale inferius (Li) was most frequently and on average superior to infradentale (Id) and inferior to Inc, and total vermilion height was smaller than total enamel height for all but 3 dentate females. Sublabiale was commonly positioned just superior to B point (females = 1.3 mm, males = 1.2 mm) in dentate individuals.

Nose

The largest differences between males and females were found for alar curvature width (M-F = 2.6 mm) and subalare width (M-F = 3.1 mm) among soft tissue ILDs and canine eminence width (M-F = 3.0 mm) and supracanine width (M-F = 2.9 mm) among bone ILDs.

Nasal aperture width was not significantly different between males and females, nor was it highly correlated with nose width (females, r = 0.460; males, r = 0.457). Many soft tissue bilateral ILDs were found via paired t-tests to correspond with bilateral bone ILDs. Alar curvature width had similar associations with supracanine width in both sexes: female alar curvature width was 1.7 mm larger and not significantly different whereas male alar curvature width was 1.6 mm larger but significantly different. Male alar curvature width was not significantly different from distal canine width at 0.3 mm smaller. Superior alar curvature width in females was not significantly different from supracanine width, but it averaged 0.7 mm smaller in width (compare to alar curvature width above); in males it was significantly smaller than supracanine width by 1.8 mm. In females subalare width was 0.2 mm smaller and the bulb width was 0.6 mm larger than nasal aperture width; in males subalare width was significantly larger averaging 2.6 mm wider and bulb width was 1.6 mm larger. For both males and females, the width between the left and right columella points was not significantly different from nasale superius width (females mean diff = -0.5 mm; males mean diff = -0.3 mm).

The position of the alar curvature point was similar for males and females, at 1.9 mm superior to nasospinale for both and 1.2 mm (females) and 1.4 mm (males) anterior to subspinale. The central columella point was 1.4 mm inferior to ANS for both males and females. Subnasale averaged 0.9 mm inferior to Ssp in females and 0.5 mm superior to subspinale in males. Pronasale averaged 1.0 mm inferior to left alare in females and 1.2 mm inferior to left alare in males, although this position varied widely from 12.1 mm inferior to 6.5 mm superior. Individuals with inferior nasal conchae that were very low within the nasal aperture had more superiorly directed nose tips. In profile view, the projection of pronasale from rhinion paralleled the contour of the nasal bones, except when a “bump” was identified posterior to rhinion,

resulting in a more inferior angle to pronasale. Regressions for predicting pronasale were generated for 2D or 3D facial approximation, as well as to accommodate damage to Rh. The strongest predictors are presented in Table 3, notably showing the strongest association between Pronasale projection from basion with distances from basion to nasal aperture points.

Table 3. Regression equations for predicting Prn'.

	Predict	Bone	r	r^2	SE	Equation
3D	Prn'-Ba	Ba-Rh	0.932	0.869	2.715	1.961 + 1.130*(Ba-Rh)
	Prn'-Ba	ANS-Ba	0.927	0.859	2.799	15.078 + 1.126*(ANS-Ba)
	Prn'-Ba	NAB-Ba	0.924	0.853	2.857	13.782 + 1.234*(Ba-NAB)
	Prn'-Ba	AlL-Ba	0.903	0.815	3.210	11.078 + 1.268*(AlL-Ba)
	Prn'-Rh	ANS-Rh	0.839	0.704	2.440	-6.434 + 1.128*(ANS-Rh)
	Prn'-Rh	Rh-Ssp	0.834	0.696	2.475	-7.053 + 0.979*(Rh-Ssp)
y-axis	Prn'_y-PoL_y	ANS_y-PoL_y	0.927	0.860	2.814	15.355 + 1.129*(ANS_y-PoL_y)
	Prn'_y-MsL_y	ANS_y-MsL_y	0.925	0.856	2.321	15.832 + 1.112*(ANS_y-MsL_y)
yz	Prn'_{yz}-Rh_{yz}	Rh_z-ANS_z	0.859	0.738	2.287	-3.620 + 1.074*(Rh_z-ANS_z)

VI. Implications for Criminal Justice Policy and Practice in the United States

The results of this study, including the quantitative data, qualitative analyses relative to traditional facial approximation guidelines, and the 3D models themselves, constitute the first comprehensive craniofacial reference datasets for practitioners in the United States. Our findings indicate that more objective estimations of facial features dimensions are possible. Further, indicators that were more defined by anatomical indicators were identified which will result in improved estimations of individualizing facial feature dimensions and positions compared to current facial approximation guidelines. Positional data between bone and skin landmarks 1) provide predictors when measurements cannot be collected, 2) can also serve as "checks" on predicted facial feature positions, and 3) contribute to guidelines for craniofacial superimposition. We have produced numerous resources, including 3D skull and face models in standard, widely viewable file formats, dense FTDMs and the open-source method for generating them and interacting with them, positions of skin landmarks relative to bone landmarks, tools for

standardizing 3D head orientation, numerous presentations, as well as guides for viewing and interacting with our dataset, including a 3D viewer based on 3DHOP [12] that opens within a web browser and requires no software installation (Figure 5). Conference presentations have been made at the American Academy of Forensic Sciences, International Association for Identification, and American Association of Physical Anthropologists and are available for download at Figshare [13] [14] [15] [16]. Tools and resources will be deployed online as well as through workshops. We have also begun applying data to facial approximations of unidentified cases in the U.S.

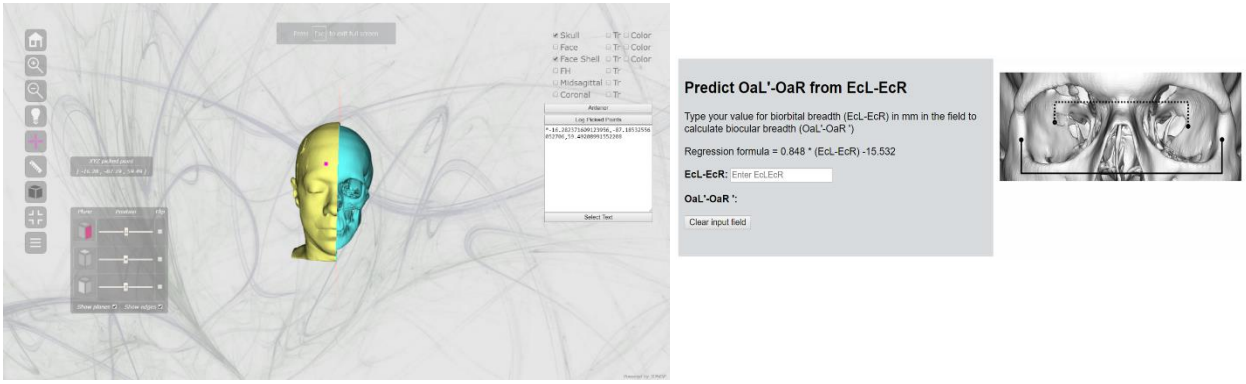

Figure 5. 3D viewing app for web browser and web-based regression calculators. HTML documents and viewers will be linked to allow toggling between 3D, regressions, qualitative observations, and data and will comprise the visual reference.

References

[1] K. Clark, B. Vendt, K. Smith, J. Freymann, J. Kirby, P. Koppel, S. Moore, S. Phillips, D. Maffitt, M. Pringle, L. Tarbox and F. Prior, "The Cancer Imaging Archive (TCIA): Maintaining and Operating a Public Information Repository," *Journal of Digital Imaging*, pp. 1045-1057, 2013.

[2] W. Bosch, W. Straube, J. Matthews and J. Purdy, *Data from Head-Neck_Cetuximab*, The Cancer Imaging Archive, 2015.

[3] R. Beichel, E. Ulrich, C. Bauer, A. Wahle, B. Brown, T. Chang, K. Plichta, B. Smith, J. Sunderland, T. Braun, A. Fedorov, D. Clunie, M. Onken, J. Riesmeier, S. Pieper, R. Kikinis, M. Graham, T. Casavant, M. Sonka and J. Buatti, *Data from QIN-HEADNECK*, The Cancer Imaging Archive, 2015.

[4] A. Fedorov, D. Clunie, E. Ulrich, C. Bauer, A. Wahle, B. Brown, M. Onken, J. Riesmeier, S. Pieper, R. Kikinis, J. Buatti and R. Beichel, "DICOM for quantitative imaging biomarker development: a standards

This resource was prepared by the author(s) using Federal funds provided by the U.S. Department of Justice. Opinions or points of view expressed are those of the author(s) and do not necessarily reflect the official position or policies of the U.S. Department of Justice.

based approach to sharing clinical data and structured PET/CT analysis results in head and neck cancer research," *PeerJ,* vol. 4, p. e2057, 2016.

[5] M. Zuley, R. Jarosz, S. Kirk, Y. Lee, R. Colen, K. Garcia, ... and N. Aredes, *Radiology data from The Cancer Genome Atlas Head-Neck Squamous Cell Carcinoma [TCGA-HNSC] collection,* The Cancer Imaging Archive, 2016.

[6] S. Kirk, Y. Lee, C. Roche, E. Bonaccio, J. Fillippini and R. Jarosz, *Radiology data from The Cancer Genome Atlas Thyroid Cancer [TCGA-THCA] collection.,* 2016.

[7] P. Cignoni, M. Callieri, M. Corsini, M. Dellepiane, F. Ganovelli and G. Ranzuglia, "MeshLab: an open-source mesh processing tool," in *Sixth Eurographics Italian Chapter Conference, pp 129-136,* 2008.

[8] T. Simmons-Ehrhardt, C. Skory Falsetti, A. Falsetti and C. Ehrhardt, "Fileset: Procedure for transforming 3D computed tomography (CT) skull and face models to a common orientation. figshare.," 2017. [Online]. Available: https://doi.org/10.6084/m9.figshare.4924694.v1. [Accessed 25 May 2017].

[9] T. Simmons-Ehrhardt, C. Falsetti, A. Falsetti and C. Ehrhardt, "User Guide: Dense facial tissue depth mapping of 3D CT models using Meshlab".

[10] T. Simmons-Ehrhardt, C. Falsetti, A. Falsetti and C. Ehrhardt, "Open-source tools for dense facial tissue depth mapping (FTDM) of computed tomography models (accepted)," *Human Biology,* 2018.

[11] O. Hammer, D. Harper and P. Ryan, "PAST: Paleontological Statistics Software Package for Education and Data Analysis," *Palaeontologia Electronica,* vol. 4, no. 1, p. 9, 2001.

[12] M. Potenziani, M. Callieri, M. Dellepiane, M. Corsini, F. Ponchio and R. Scopigno, "3DHOP: 3D Heritage Online Presenter," *Computers & Graphics,* vol. 52, pp. 129-141, 2015.

[13] T. Simmons-Ehrhardt, C. Skory Falsetti and C. Ehrhardt, *Innovative uses of CT scans for the enhancement of forensic facial approximation methods: a collaboration between forensic science researchers and facial approximation practitioners,* Cincinnati, OH: Figshare, 2016.

[14] T. Simmons-Ehrhardt, C. Skory Falsetti and C. Ehrhardt, *Craniofacial analysis of 3D computed tomography (CT) models and a new method for dense facial tissue depth mapping: a collaboration between forensic science researchers and forensic art practitioners,* Las Vegas, NV: Figshare, 2016.

[15] T. Simmons-Ehrhardt, C. Skory Falsetti, A. Falsetti and C. Ehrhardt, *Enhancing craniofacial identification methods with CT data,* Austin, TX: Figshare, 2018.

[16] A. Falsetti, T. Simmons-Ehrhardt, C. Falsetti and C. Ehrhardt, *Facilitating practitioner interaction with 3D craniofacial identification resources,* Austin, TX: Figshare, 2018.